Article

Water Adsorption on the β-Dicalcium Silicate Surface from DFT Simulations

Qianqian Wang,[1] Hegoi Manzano,[2]* Iñigo López-Arbeloa,[3] and Xiaodong Shen [1]*

[1] State Key Laboratory of Materials-Oriented Chemical Engineering, College of Materials Science and Engineering, Nanjing Tech University, Nanjing 210009, China.
[2] Condensed Matter Physics Department, University of the Basque Country, UPV/EHU, 48080, Bilbao, Spain
[3] Molecular Spectroscopy Laboratory, Department of Physical Chemistry, University of the Basque Country, UPV/EHU, 48080, Bilbao, Spain

* Correspondence: hegoi.manzano@ehu.eus, xdshen@njtech.edu.cn

Abstract: *β*-dicalcium silicate (*β*-Ca_2SiO_4, or *β*-C_2S in cement chemistry notation) is one of the most important minerals in cement. An improvement of its hydration rate would be the key point for developing environmentally friendly cements with lower energy consumption and CO_2 emissions. However, there is a lack of fundamental understanding on the water/β-C_2S surface interactions. In this work we aim to evaluate the water adsorption on three *β*-C_2S surfaces at the atomic scale using density functional theory (DFT) calculations. Our results indicate that thermodynamically favorable water adsorption takes place in several surface sites, with a broad range of adsorption energies (−0.78 to −1.48 eV), depending on the particular mineral surface and adsorption site. To clarify the key factor governing the adsorption, the electronic properties of water at the surface were analyzed. The partial density of states (DOS), charge analysis, and electron density difference analyses suggest a dual interaction of water with *β*-C_2S (100) surface: a nucleophilic interaction of the water oxygen lone pair with surface calcium atoms, and an electrophilic interaction (hydrogen bond) of one water hydrogen with surface oxygen atoms. Despite the elucidation of the adsorption mechanism, no correlation was found between the electronic structure and the adsorption energies.

Keywords: Belite, Hydration, Density Functional Theory, Water Adsorption, Calcium Silicate

1. Introduction

Hydration and dissolution of crystals have a profound impact on a broad range of scientific and technological processes such as thermochemical energy storage [1,2] , geochemical phenomena at the mineral/water interfaces [4,5], and durability of glasses and biomaterials [6]. A prominent technological application of crystal dissolution is the production of cement and concrete. Cement, as the "adhesive" in concrete, is used worldwide in social infrastructures, military and civil buildings, being the most consumed manufactured material. The clinker hydration is the crucial step which controls the final properties of cement materials, and yet, the hydration process of cement minerals are still arguably despite the long lasting research [7]. Due to the large amount of CO_2 emissions and energy consumption in cement industry and the increasing demand, understanding cement hydration mechanisms is urgently needed to supply an academic basis for the design of new environmentally friendly cements. A great candidate to achieve this objective is Belite. Belite (*β*-dicalcium silicate, *β*-C_2S in cement chemistry notation) is an artificial orthosilicate that forms during the sintering of cement clinker, yet it has a natural counterpart called Larnite [8] that appears in

Preprints (www.preprints.org) | NOT PEER-REVIEWED | Posted: 2 August 2018 doi:10.20944/preprints201804.0080.v2

natural environments. It is one of the most important minerals in cement industry, and has potential advantages for achieving the low carbon emission goal due to its lower sintering temperature and low calcium carbonate resource demanding compared to tricalcium silicate, the base component of traditional cements. However, the low hydration rate of belite restricts its engineering applications. Until now, the experimental endeavours conducted to improve its hydration [9-12] have had a very limited success.

In such scenario, atomistic simulations are a valuable tool as a complement to experiments in order to study the hydration mechanism of materials, as they have demonstrated for ionic solids [13], metallic oxides[14, 15] , minerals [16–18], or ceramics . Regarding cement, atomistic simulations have been mainly used to investigate tricalcium silicate [20–26], the main component of cement, and much less attention has been paid to β-C_2S [27–29]. In this article we aim to investigate the interaction between β-C_2S surface and water molecules from a fundamental point of view, using Density Functional Theory (DFT) simulations. While dissolution is a very complex problem influenced by many microscopic and macroscopic factors that are not taken into account, the atomic scale interaction is the first step that will determine dissolution. Therefore, the results obtained here will help us to understand some fundamental factors that govern β-C_2S/water interaction.

2. Materials and Methods

2.1. Model Construction

The crystal structure of β-C_2S resolved by Mumme [30] was used as the starting point. Based on previous DFT studies [27,28], we decided to use the (100), (101) and (010) surfaces to investigate the water dissociation process. Analyzing the crystal Wulff's crystal reconstruction, showed in the appendix A, we observed that the contribution of these three surfaces to the equilibrium shape's total surface area is nearly the same, ~ 20%, and hence, together they account for 60% of the total crystal's surface. The three surfaces were cleaved trough an appropriate plane to generate Tasker type I slabs, i.e. symmetrical surfaces without macroscopic dipolar moments that lead to spurious results and inestabilities. The dipole neutrality can be checked by looking at the the projection of the electrostatic potential along the perpendicular direction to the surfaces showed in Fig 1.. For the three surfaces the electrostatic potentials of the upper and bottom surfaces are symmetrical, with a considerable change at the interface where it becomes wider as it extends to the vacuum region. In the middle of vacuum layer, the electrostatic potential matches the vacuum level energy, which indicates that there is no interaction between the upper and lower surfaces. Therefore, the vacuum layer thickness is enough to avoid self-interactions and the net dipole moment is zero in the three slabs. The final area and thickness of the slabs with dimensions are shown in Table 1.

Table 1. Summary of the properties for the studied surfaces.

Surface index	Slab size (Å)	Thickness of the Slab(Å)	Surface Energy (J m^{-2})	Contribution to the Wulf Shape
(100)	13.5 x 9.3	16.3	0.85	18%
(010)	9.3 x 11.0	20.4	1.00	19%
(101)	11.2 x 13.5	19.0	0.76	21%

2.2. Computational details

The DMol3 density functional theory (DFT) package [31] was employed to study the interaction between the slab model and water. The exchange-correlation is treated in the generalized gradient

Preprints (www.preprints.org) | NOT PEER-REVIEWED | Posted: 2 August 2018 doi:10.20944/preprints201804.0080.v2

approximation (GGA) with the Perdew-Burke-Ernzerhof (PBE) functional [32]. The treatment for the core electrons is all electrons method. A double ζ plus polarization (DZP) basis set is used, with a global orbital cut-off radius of 5.5 Å. The orbital smearing parameter is set to 0.01 eV to balance precision and computing performance. The k-point grid in the first Brillouin zone is constructed using the Monkhorst-Pack method [33], with a 2×2×1 k-points grid. Self-consistent iteration convergence precision is set to 2.5×10^{-5} eV, the energy convergence tolerance to 2.5×10^{-4} eV, and the maximum stress is set to be lower than 0.05 eV/Å. During surface relaxation process a maximum displacement of atoms of 0.005 Å at each step was allowed, and the middle of slab (6.5 Å from each surface) atoms were fixed.

The adsorption energies are computed placing a single water molecule above the surface at an initial distance of ~ 2 Å. The surface sites were chosen based on a surface sampling of the adsorption energies done at the empirical level with ReaxFF [28]. One the configurations were set, an energy minimization was done at the DFT level, and the adsorption energy was computed with the following expresion:

$$\boldsymbol{E_{ads} = \left(E_{slab} + E_{H_2O}\right) - E_{H_2O@slab}}$$

so the more negative the value, the more favorable the adsorption site. Furthermore, an external additional potential was applied to correct macroscopic dipole formation when water molecules are present [34].

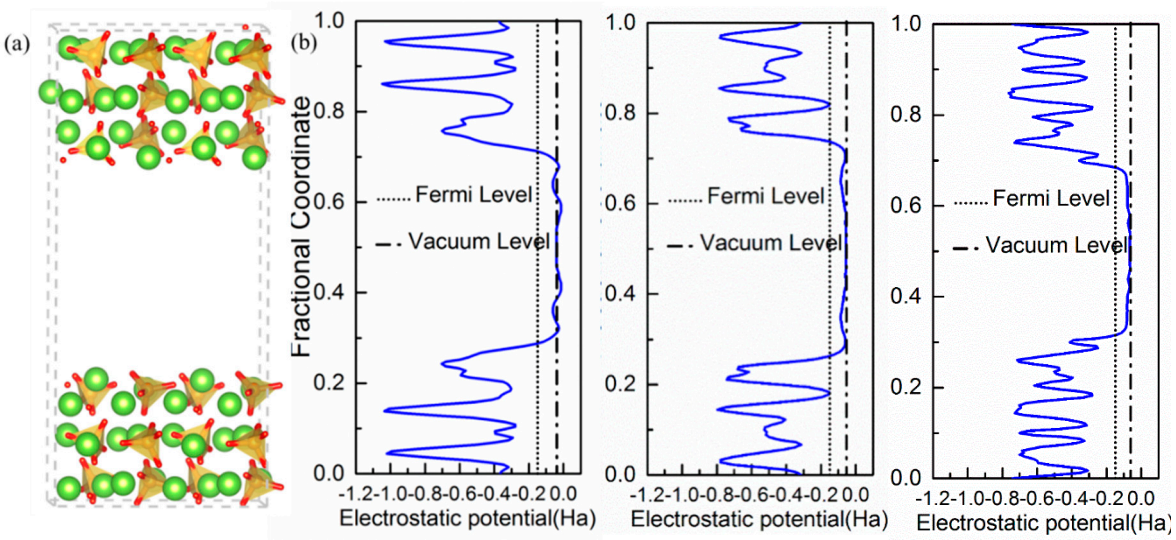

Figure 1 (a) Atomic representation of the *β*-C_2S (100) surface model visualized with VESTA[35]. Red, green and orange spheres represent oxygen, calcium and silicate atoms, respectively. The SiO_4^{-4} groups are further represented as orange tetrahedra. **(b)** Electrostatic potentials along with the vertical vectors of the slab for the (100), (101) and (010) cleavage directions. The solid line represents the vacuum level.

3. Results

3.1. Water adsorption conformation on β-C2S (100) surface and bonding scheme

The surface structure of β-C_2S is quite irregular, with Ca and O ions of different symmetry present, silicate ions arranged with different orientations, and a considerable roughness. Therefore, it is more difficult to define "a priori" the water adsorption points on the surface than for symmetrical

Preprints (www.preprints.org) | NOT PEER-REVIEWED | Posted: 2 August 2018 doi:10.20944/preprints201804.0080.v2

metal oxides, such as TiO_2, CaO , MgO [14,36,37], or two-dimensional materials, such as Ti_2C [19]. In a previous work [28], water adsorption sites were exhaustively searched using empirical force field simulations for the (100) surface. Using that information, we have targeted the most favourable adsorption sites of water at β-C_2S, performing an energy minimization on the force field final configuration for each adsorption configuration. The process has been repeated for the (010) and (101) surfaces.

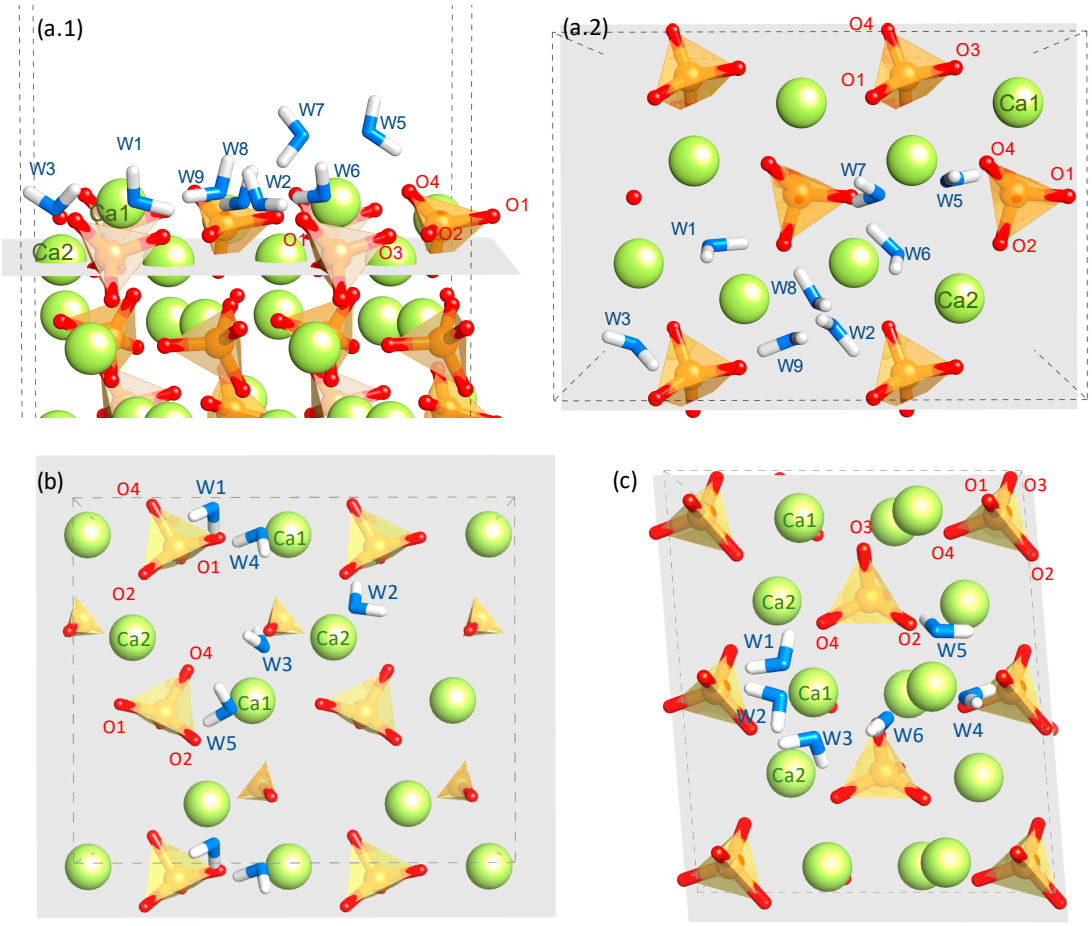

Figure 2 . (a) Water adsorption configurations on β-C_2S (100) in side (a.1) and top (a.2) views. For the β-C_2S (101) (b) and (010) (c) only the top view is shown. The nomenclature of the Ca and O sites from dicalcium silicate follow that of the original paper describing the crystalline structure [30]. The atoms representation is the same as in figure 1, including the water molecules with the O atoms in blue and the H atoms in white. It must be noted that the conformation sites labelled as W2 and W4 in the (100) were different in the empirical simulation, yet after the present DFT energy minimization they became equivalent.

The investigated sites are shown in Fig. 2, and the corresponding adsorption energies in Table 1. In general, water is adsorbed in a configuration with the oxygen atom O(w) coordinated to surface calcium atoms Ca, and one of its hydrogen atoms H(w) pointing towards the surface, forming a hydrogen bond with oxygen atoms O(s) from the surface silicate groups. The adsorption energies vary in a range from -0.78 to -1.47 eV, which indicates that the surfaces are considerably hydrophilic and adsorption energetically favourable [38]. The dispersion in the adsorption energy for each surface and the comparison with other orthosilicates will be discussed in section 4. In all the reported adsorption sites the water molecule establishes a single hydrogen bond with O(s) atoms, with bond lengths smaller than 1.75 Å and H(w)-O(w)-O(s) angles below 24º. In water, hydrogen bond distances

Preprints (www.preprints.org) | NOT PEER-REVIEWED | Posted: 2 August 2018 doi:10.20944/preprints201804.0080.v2

and angles are typically larger, about 1.9 Å and less than 35º respectively [39,40]. Since the hydrogen bond length and strength are usually correlated [39] this suggests a strong hydrogen bond between water and belite surface. Regarding the Ca-O(w) distance, we found that the coordination distances of Ca-O(w) on the interface are bellow 2.8 Å which match with the Ca-O coordination distance on bulk β-C_2S [30].

Based on the described conformations we can suggest a bonding scheme in which β-C_2S suffers simultaneously both nucleophilic and electrophilic attack from water [22,29]: the Ca is an electron acceptor from the O(w) electron donor, and the O(s) is an electron donor (or proton acceptor) to the H(w) electron acceptor, forming a hydrogen bond. However, it is quite complex to correlate the magnitude of the adsorption energy as a function of the conformation adopted by water at the surface. Hence, it is necessary to analyse the electronic properties of the adsorbate/substrate system to understand the water adsorption mechanism on the surface.

Table 2. Hirshfeld charge of water molecule atoms for various adsorption sites as well as the corresponding adsorption energies. The adsorption sites are name in descending adsorption energy order, and the surface Ca and oxygen numbers are thos in figure 2. The water molecule atoms are named with the w subscript. The H_w taking part of the hydrogen bond (see text) is labeled as H_w (O)

	Adsorption Site	Adsorption energy (eV)	Hirshfeld charge on water (e-)				Hirshfeld charge on surfaces (e-)		Bond distance Ca-Ow (Å)	Bond distance O-Hw (Å)
			Ow	Hw(O)	Hw	Total	Ca	O		
H_2O	-	-	-0.302	0.151	0.151	0	-	-	-	-
(100)										
W1	Ca1 O4	-1.24	-0.198	0.099	0.180	0.081	0.612	-0.321	2.595	1.419
W2	Ca2 O3	-1.14	-0.195	0.108	0.181	0.094	0.477	-0.361	2.644	1.598
W3	Ca2 O3	-1.14	-0.196	0.107	0.179	0.09	0.475	-0.362	2.630	1.593
W4	Ca2 O3	-1.14	-0.198	0.106	0.179	0.087	0.476	-0.362	2.630	1.392
W5	Ca1 O2	-1.09	-0.269	0.101	0.169	0.001	0.649	-0.356	2.351	1.550
W6	Ca2 O1	-1.07	-0.218	0.095	0.176	0.053	0.446	-0.218	2.542	1.393
W7	Ca1 O1	-1.00	-0.258	0.108	0.174	0.024	0.649	-0.258	2.395	1.661
W8	Ca2 O4	-0.91	-0.203	0.103	0.177	0.077	0.462	-0.203	2.560	1.524
W9	Ca1 O1	-0.78	-0.207	0.122	0.182	0.097	0.498	-0.207	2.546	1.677
(101)										
W1	Ca2O1	-0.974	-0.266	0.103	0.162	-0.001	0.5043	-0.3559	2.481	1.604
W2	Ca2O2	-0.932	-0.266	0.1075	0.1648	0.006	0.4989	-0.3599	2.499	1.665
W3	Ca1O3	-0.922	-0.226	0.1156	0.1697	0.06	0.5219	-0.325	2.781	1.568
W4	Ca1O1	-0.921	-0.256	0.1038	0.1619	0.01	0.4930	-0.3499	2.522	1.553
W5	Ca1O2	-0.853	-0.262	0.1026	0.1609	0.002	0.4936	-0.3591	2.519	1.603
(010)										
W1	Ca1O1	-1.477	-0.278	0.0957	0.1392	-0.043	0.5029	-0.3882	2.431	1.612
W2	Ca1O1	-1.430	-0.272	0.0949	0.1613	-0.016	0.4928	-0.3869	2.448	1.580
W3	Ca1O4	-1.365	-0.258	0.1073	0.163	0.012	0.5084	-0.3601	2.463	1.726
W4	Ca2O1	-1.199	-0.273	0.0992	0.1641	-0.001	0.5587	-0.3883	2.383	1.558
W5	Ca2O2	-1.094	-0.272	0.1054	0.1492	-0.01	0.5856	-0.3544	2.498	1.731
W6	Ca2O3	-1.044	-0.252	0.1121	0.1723	0.032	0.5623	-0.3458	2.421	1.658

 doi:10.20944/preprints201804.0080.v2

3.2. Charge population analysis

A Hirshfield population analysis [41] was performed to investigate the atomic charge transfer between the water molecule and the surface. Table 2 gives the computed charges on the water molecule atoms for the adsorption sites as well as the charges on the surface atoms. Compared with the isolated water molecule, the absolute values of the Hirschfeld charges on the water oxygen atoms have decreased in all the adsorption configurations. It suggests electron transfer from O(w) to Ca(s) as we proposed before. Regarding the water hydrogen atoms, we can first observe an anisotropy in their charges, due to the formation of a single hydrogen bond between a water and surface oxygen atom. The H(w) involved in the hydrogen bond is an electron acceptor from the surface O(s), therefore decreasing its positive charge from 0.151 to an average value of 0.105. The remaining hydrogen, pointing towards the vacuum, increases its charge to, possible due to intramolecular electron withdraw from the O(w) which has donate electrons to the surface. The trend of the Hirshfeld population on the β-C_2S (100) surface atoms involved in the adsorption corroborate the changes described for the water molecules. There is a positive charge decrease on Ca(s) due to the electron transfer from O(w), and a negative charge decrease on the O(s) due to the electron transfer to the H(w).

The Hirshfeld population analysis interpretation matches with the proposed bonding scheme. Depending on the specific adsorption site, there is a net positive or negative charge on the adsorbed water molecule. A positive charge indicates that the electron depletion of the O(w) donnor is more important that the electron surfeit of the H(w), and a negative charge the opposite. Hence, the population analysis suggests that the main interaction in the water adsorption can be the O(w)-Ca ionic interaction or the hydrogen bond depending on the specific site. If we compare the binding energy when the hydrogen bond is the main contribution with the one in bulk water, 0.22 eV [42,43], we can suggest that the water/surface is considerable stronger than a typical water-water interaction.

3.3. Partial Density of States

Hirshfeld population analysis reveals a net electron transfer from the water molecules to the surface. For further understanding of the process, the partial density of states (PDOS) of the Ca(s) and O(s) atoms involved in the highest adsorption energy site (W1) and the lowest adsorption energy site (W9) are presented in Fig. 3, before and after water adsorption. Fig. 3 shows only the results for the (100) surface, yet the behaviour is the same for the other two studied cleavages, and the PDOS are included in appendix B.

In both sites, the p-orbitals from surface O atoms are the most significant states contributing to the valence band maximum (VBM). This indicates that the under coordinated dangling oxygen atoms on the surface localize the electronic charge, being susceptible for suffering electrophilic attack from water and donate electrons. Regarding the conduction band minimum (CBM), there is a larger contribution of Ca1-s unoccupied states in the of W1 and W9 sites. Hence, the surface Ca atoms are prone of suffering nucleophilic attack and accept electrons. Therefore, the PDOS of the bare surface matches again with the suggested bonding scheme. Overall, the contribution of oxygen p-states to the VBM and the calcium s-states to the CBM is stronger in the W1 sites, which makes them more favorable both for electrophilic and nucleophilic attack, a perfect situation for the adsorption of water molecules, as can be seen from its corresponding adsorption energy.

After water chemisorption, the orbitals of the water molecule are hybridized with both O-p VBM and Ca-s CBM states of the surfaces as shown in fig. 3(c) and (d), respectively. Furthermore, in the W1 site the CBM is distributed both in the Ca-s and H(w) unoccupied states, while in the W9 it is strongly localized in the water hydrogen atoms. This suggests that the H(w) in the W9 has not established a strong hydrogen bond with the O(s), and therefore still has the capacity to accept electrons. In fact, the Hirsfeld charge on the H(w) at the W9 site has suffer the lower decrease with

Preprints (www.preprints.org) | NOT PEER-REVIEWED | Posted: 2 August 2018 doi:10.20944/preprints201804.0080.v2

respect to the isolated water, confirming this interpretation. Again, these findings agree with the bonding scheme proposed from previous analysis, and give an explanation of the more favourable water adsotpion in W1 than W9 sites.

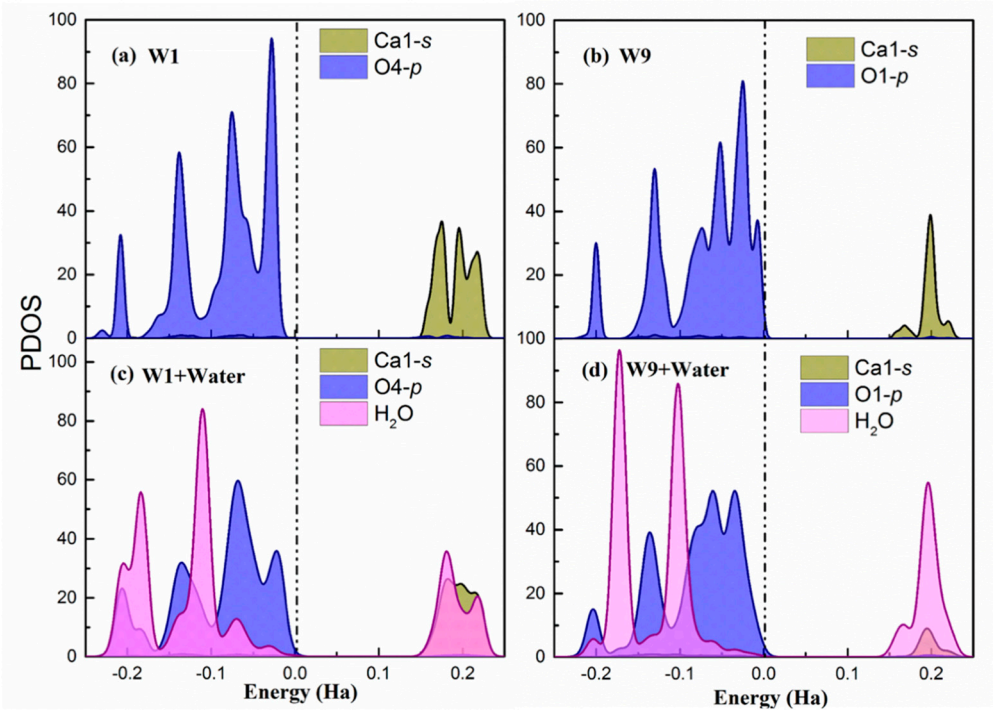

Figure 3. (a) and (b) The partial density of states of W1 and W9 adsorption sites on the relaxed surface; (c) and (d) The partial density of states of W1 and W9 adsorption sites after water adsorbed on the surface. The dash dot line indicates the Fermi level. Note that Ca1 in sites W1 and W9 were equivalent in the bulk but after slab relaxation they are innequivalent and hence theri different PDOS.

3.4 Chemical bonding from charge density difference analysis

To complete the characterization of chemical bonding and charge transfer, we move forward to study the spatial electron density distribution before and after the water adsorption from electron density difference, Δρ, calculated from the formula:

$$\Delta\rho = (\rho_{H_2O} + \rho_{surf}) - \rho_{H_2O+surf} \quad (1)$$

where $\rho_{H2O+surf}$ represents the electron density distribution of the water adsorbed on the surface; ρ_{H2O} and ρ_{surf} are the electron densities of individual water molecules and pure surface respectively. Accordingly, a positive Δρ value in a point indicate a lower electronic density after water adsorption due to electron density depletion, and negative values a higher electronic density due to electron density surfeit. The electron density difference was plotted in Fig. 4, where light and dark blue isosurfaces represent the $\Delta\rho < 0$ and > 0 respectively.

It can be observed that the electron density around the adsorption points of the surface is significantly polarized after the water adsorption, yet the effect is local and only the atoms involved in the adsorption site are affected. In both cases the situation is similar: there is a localized electronic density depletion in the O(s) atoms that forms the hydrogen bond, as well as a more delocalized depletion in the area of the water oxygen lone pair. On the other hand, the electronic density increment on the H(w) atoms, and the Ca(s) atoms shown in Fig. 4(c) and 4(d). It must be noted that the electron density surfeit takes place in more than one Ca atoms from the surface, so the adsorption site involves an ionic interaction with more than one Ca atom from the surface. From the charge density isosurfaces, it is apparent that the charge transfer is more pronounced on the W1 sites in

Preprints (www.preprints.org) | NOT PEER-REVIEWED | Posted: 2 August 2018 doi:10.20944/preprints201804.0080.v2

comparison with the W9 sites, which is in agreement with the Hirshfeld populations, the PDOS analysis, and the computed adsorption energies.

Once more, the findings are consistent with the suggested electrophilic-nucleophilic dual adsorption scheme, i.e., the H(w) being an electron acceptor from the surface O and the O(w) being an electron donor to surface Ca atoms.

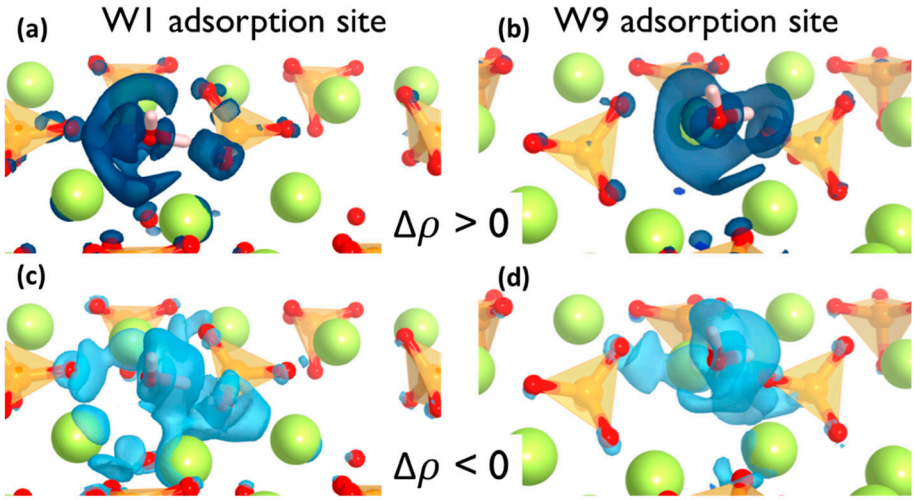

Figure 4. Isosurface plots of the electron density difference for W1 (a,c) and W9 (b,d) adsorption sites. Dark and light blue isosurfaces indicate the electron density depletion and surfeit, respectively.

4. Discussion

The "results" section has been focused on a detailed description of the electronic nature of the water adsorption on three β-belite surfaces. The basic mechanism consists on a simulateneous nucleophilic and electrophilic interaction of water oxygen and hydrongen atoms with the β-C2S calcium and oxygen atoms respectively. However, we could not find a clear correlation between the electronic structure, atomic charges, adsorption configuration and adsorption energies. To gain a useful insight it is interesting to compare the adosrption energies between different surfaces and with other related minerals.

The water adsorption energy on the three studied surfaces are within the same range, always favourable. There is no apparent correlation with their surface energies, and the adsorption energies on the (101) are more homogeneous than in the (100) and (010) yet again no clear reason was found. Nevetheless, we could conclude that among the studied surfaces there is not a preferent one, and the attack of water to β-C2S may be homogeneous.

The adsorption energies can be compared with those reported by DFT for the olivine family of orthosilicates by Kerisit et al. [44]. These results correspond to the adsorption energy of a single water molecule adsoprtion per unit cell in two configurations, flat and side, always in the (010) surface. For the olivine family different adsorption energies were found depending on the cation increasing following the serie Mn < Fe < Co < Ca ≈ Mg. First, it must be pointed out that the DFT adsroption energies from Kerisit et al. do not follow the same trend as the experimental dissolution rates [3], which suggests that water adsoption energies are just a small portion of the complex process that is dissolution. Second, it is clear that our results are in the same range of other orthosilicates. It is noteworthy that calcium olivine is the one with a larger difference of adsorption energies, which is consistent with the dispersion that we found in our study. Finally, it must be noted that the

Preprints (www.preprints.org) | NOT PEER-REVIEWED | Posted: 2 August 2018 doi:10.20944/preprints201804.0080.v2

comparison with olivines is very relevant from the cement perspective because calcium olivine mineral is the γ-polymorph of belite, a phase that is avoided in cement production due to its negligible reactivity. Comparing our results with those of Kerisit, it seems that the γ-polymorph presents larger water adsorption energies than the β-polymorph, a counterintuitive result that was previously reported in [28], becasue the experimental dissolution rate of β-C2S is larger than that of γ-C2S.

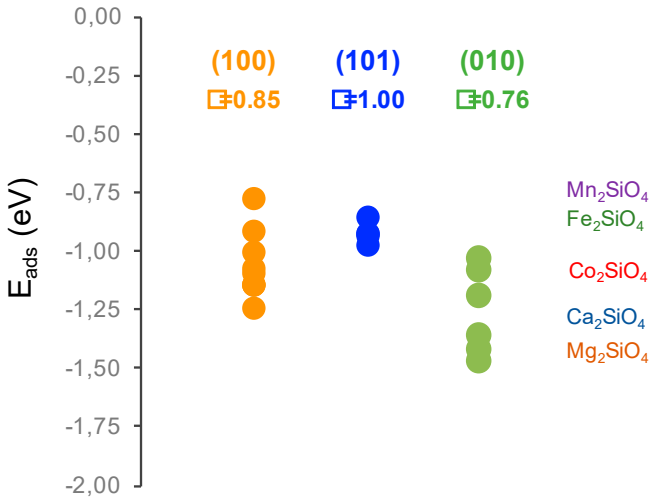

Figure 5. Adsorption energies of water on β-belite surfaces compared to the values reported with DFT for the olivine orthosilicate family [44].

5. Conclusions

β-dicalcium silicate is a promising candidate to develop low-CO_2 cements, yet its slow hydration rate has limited its practical applications so far. In this work density functional theory simulations have been employed with the aim of understanding the water adsorption mechanism on β-dicalcium silicate surfaces.

Due to the structural complexity, there are multiple water adsorption sites with different energies on β-C2S surfaces. The most favorable adsorption sites are ascribed to the co-existence of a dangling oxygen atom from the silicate group and surface calcium atoms. The structural and electronic analyses point towards a double nucleophilic-electrophilic attack by water molecules to the β-C2S surfaces: On the one hand, there is electron transfer from the water molecule oxygen atom to the surface Ca atoms. On the other hand, one of the water hydrogen atoms establishes a hydrogen bond with the silicate oxygen atoms along with transferring positive charge onto the silicate oxygen atoms. The results suggest that Frenkel or Schottky and isovalent chemical substitutions of Ca or O by more electropositive and electronegative atoms should create favourable points for water nucleophilic-electrophilic dual interaction. However, it must be taken into account that the point defects will enhance local affinity for water, yet macroscopic hydration will be also influenced by line, plane, and bulk defects [7,45].

The water adsorption energies on the three studied surfaces are consistent with previous results for the olivine orthosilicate family. They lie in the same energy range, which suggests no preferential direction for water attack, and there is a considerable dispersion on the values that does not correlate with the electronic structure or adsorption configuration. Also, the inconsistency between the DFT results and the experimental dissolution rates make us suggest that DFT calculations help us to

Preprints (www.preprints.org) | NOT PEER-REVIEWED | Posted: 2 August 2018 doi:10.20944/preprints201804.0080.v2

elucidate in detail the atomic scale interaction, yet do not provide the necessary information to draw conclusion about macroscopic dissolution rates.

Acknowledgments: The authors thank the supports of the Project Funded by the National Natural Science Foundation of China (No. 51602148), the Priority Academic Program Development of Jiangsu Higher Education Institutions (PAPD), the Program for Innovative Research Team in University of Ministry of Education of China (No.IRT_15R35), the financial support from the Departamento de Educación, Política Lingüística y Cultura del Gobierno Vasco (IT912-16) and the ELKARTEK project. The technical and human support provided by IZO-SGI SGIker of UPV/EHU and European funding (ERDF and ESF) is also acknowledged.

Author Contributions: "Q.W., H.M. and X.S. conceived and designed the simulations; Q.W. performed the simulations; Q.W. and H.M. analyzed the data; Q.W., H.M. X.S. and I.L. wrote the paper."

Appendix A

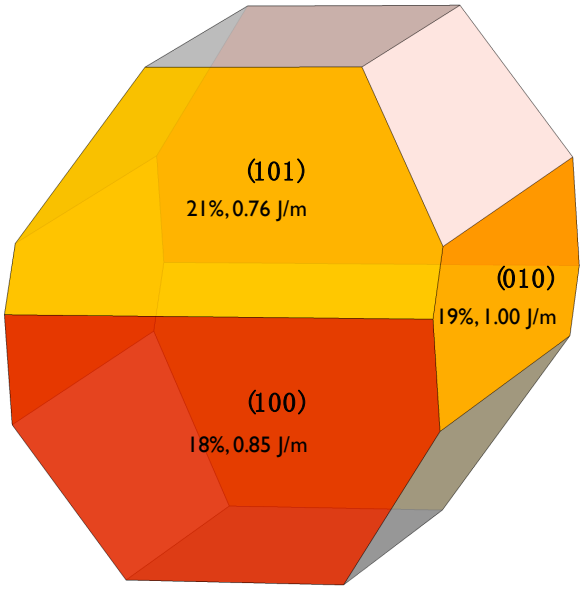

Figure S1. Wulff shape reconstruction of β-C_2S according to the surfaces energies computed in ref. [28]. The 3 studied surfaces are colored, and the label shows their cleavage, their contribution to the total surface, and their surface energies. The shape reconstruction and the contribution of each surface to the total area of the crystal has been obtained from the VESTA code [35].

Preprints (www.preprints.org) | NOT PEER-REVIEWED | Posted: 2 August 2018 doi:10.20944/preprints201804.0080.v2

Appendix B

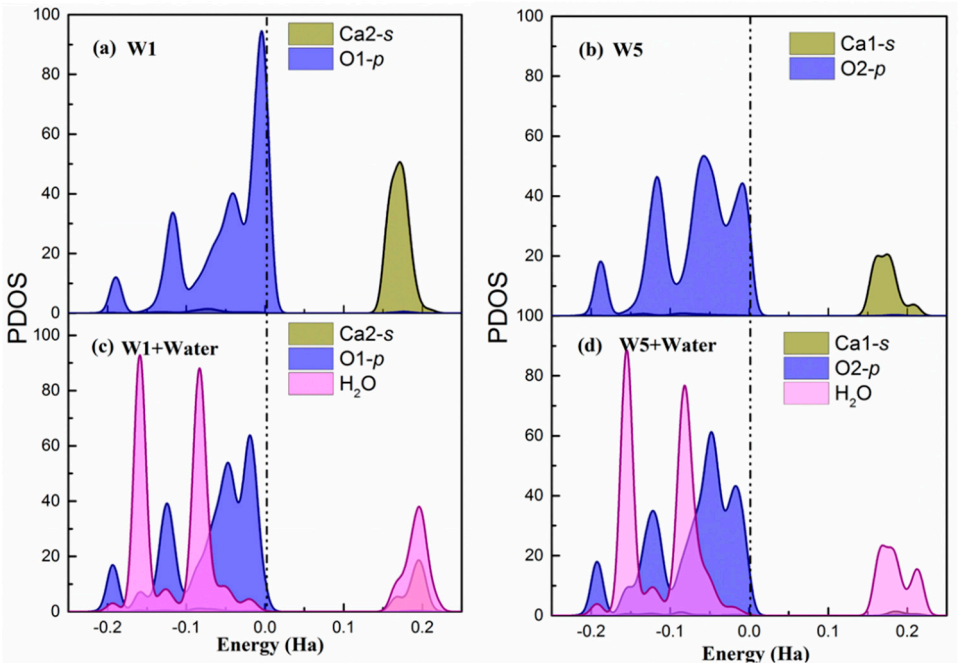

Figure S2. Surface (101) (a) and (b) The partial density of states of W1 and W5 adsorption sites on the relaxed surface; (c) and (d) The partial density of states of W1 and W5 adsorption sites after water adsorbed on the surface. The dash dot line indicates the Fermi level.

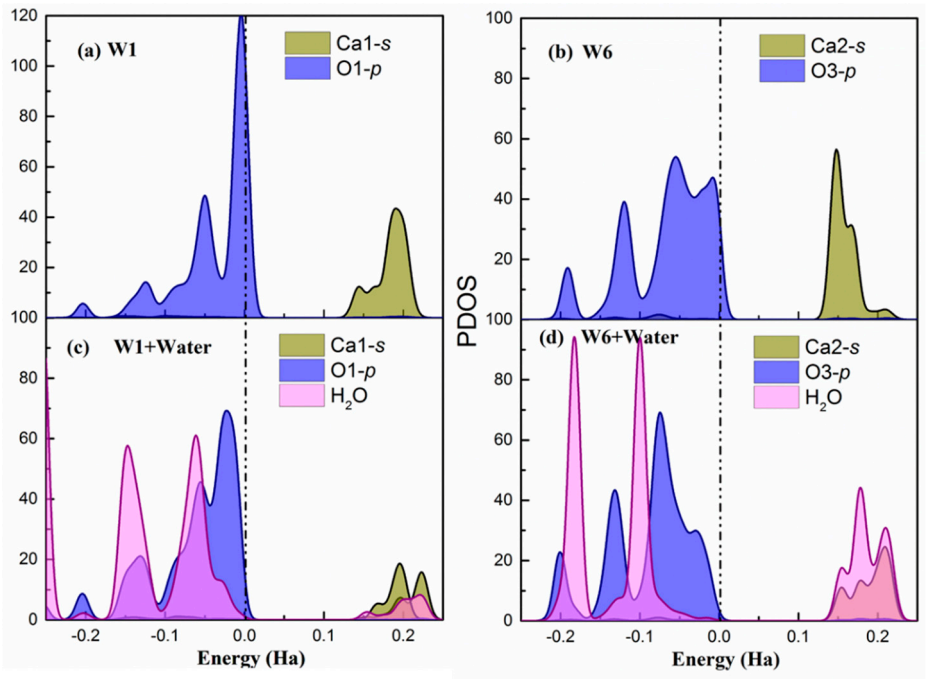

Figure S3. Surface (010) (a) and (b) The partial density of states of W1 and W5 adsorption sites on the relaxed surface; (c) and (d) The partial density of states of W1 and W5 adsorption sites after water adsorbed on the surface. The dash dot line indicates the Fermi level.

 doi:10.20944/preprints201804.0080.v2

References

1. Cot-Gores, J.; Castell, A.; Cabeza, L. F. Thermochemical energy storage and conversion: A-state-of-the-art review of the experimental research under practical conditions. *Renew. Sustain. Energy Rev.* **2012**, *16*, 5207–5224, doi:10.1016/j.rser.2012.04.007.
2. Sharma, A.; Tyagi, V. V; Chen, C. R.; Buddhi, D. Review on theermal energy storage with phase change materials and applications. *Renew. Sustain. energy Rev.* **2009**, *13*, 318–345.
3. Ohlin, C. A.; Villa, E. M.; Rustad, J. R.; Casey, W. H. Dissolution of insulating oxide materials at the molecular scale. *Nat. Mater.* **2010**, *9*, 11–9, doi:10.1038/nmat2585.
4. Brantley, S. L.; Kubicki, J. D.; White, A. F. *Kinetics of water-rock interaction*; Springer, 2008; Vol. 168;.
5. Oelkers, E. H. General kinetic description of multioxide silicate mineral and glass dissolution. *Geochim. Cosmochim. Acta* **2001**, *65*, 3703–3719, doi:10.1016/S0016-7037(01)00710-4.
6. Porter, A. E.; Patel, N.; Skepper, J. N.; Best, S. M.; Bonfield, W. Comparison of in vivo dissolution processes in hydroxyapatite and silicon-substituted hydroxyapatite bioceramics. *Biomaterials* **2003**, *24*, 4609–4620, doi:10.1016/S0142-9612(03)00355-7.
7. Bullard, J. W.; Jennings, H. M.; Livingston, R. A.; Nonat, A.; Scherer, G. W.; Schweitzer, J. S.; Scrivener, K. L.; Thomas, J. J. Mechanisms of cement hydration. *Cem. Concr. Res.* **2011**, *41*, 1208–1223.
8. Jost, K. H.; Ziemer, B.; Seydel, R.; H, K. Redetermination of structure of beta-dicalcium silicate. *Acta Crystallogr. Sect. B-Structural Sci.* **1977**, *33*, 1696–1700.
9. Fukuda, K.; Ito, S. Improvement in reactivity and grindability of belite-rich cement by remelting reaction. *J. Am. Ceram. Soc.* **1999**, *82*, 2177–2180.
10. Cuberos, A. J. M.; De la Torre, A. G.; Martin-Sedeno, M. C.; Moreno-real, L.; Merlini, M.; Ordonez, L. M.; Aranda, M. A. G.; De, Á. G.; Martín-sedeño, M. C.; Ordónez, L. M. Phase development in conventional and active belite cement pastes by Rietveld analysis and chemical constraints. *Cem. Concr. Res.* **2009**, *39*, 833–842, doi:10.1016/j.cemconres.2009.06.017.
11. Cuberos, A. J. M.; De la Torre, A. G.; Alvarez-Pinazo, G.; Martin-Sedeno, M. C.; Schollbach, K.; Pollmann, H.; Aranda, M. A. G. Active Iron-Rich Belite Sulfoaluminate Cements: Clinkering and Hydration. *Environ. Sci. Technol.* **2010**, *44*, 6855–6862, doi:10.1021/es101785n.
12. ElDidamony, H.; Sharara, A. M.; Helmy, I. M.; ElAleem, S. A. Hydration characteristics of beta-C2S in the presence of some accelerators. *Cem. Concr. Res.* **1996**, *26*, 1179–1187.
13. Yang, H. G.; Sun, C. H.; Qiao, S. Z.; Zou, J.; Liu, G.; Smith, S. C.; Cheng, H. M.; Lu, G. Q. Anatase TiO2 single crystals with a large percentage of reactive facets. *Nature* **2008**, *453*, 638–641, doi:10.1038/nature06964.
14. Manzano, H.; Pellenq, R. J. M.; Ulm, F.-J.; Buehler, M. J.; van Duin, A. C. T. Hydration of Calcium Oxide Surface Predicted by Reactive Force Field Molecular Dynamics. *Langmuir* **2012**, *28*, 4187–4197, doi:10.1021/la204338m.
15. Raymand, D.; van Duin, A. C. T. T.; Spångberg, D.; Goddard, W. a.; Hermansson, K.; Spangberg, D. Water adsorption on stepped ZnO surfaces from MD simulation. *Surf. Sci.* **2010**, *604*, 741–752, doi:10.1016/j.susc.2009.12.012.
16. Stack, A. G.; Raiteri, P.; Gale, J. D. Accurate Rates of the Complex Mechanisms for Growth and Dissolution of Minerals Using a Combination of Rare-Event Theories. *J. Am. Chem. Soc.* **2011**, *134*, 11–14, doi:10.1021/ja204714k.
17. De Leeuw, N. H.; Parker, S. C. Molecular-dynamics simulation of MgO surfaces in liquid water using a shell-model potential for water. *Phys. Rev. B* **1998**, *58*, 13901–13908, doi:10.1103/PhysRevB.58.13901.
18. de Leeuw, N. H.; Parker, S. C.; Catlow, C. R. a.; Price, G. D.; Leeuw, N. H. De Modelling the effect of water

on the surface structure and stability of forsterite. *Phys. Chem. Miner.* **2000**, *27*, 332–341, doi:10.1007/s002690050262.

19. Cicero, G.; Grossman, J. C.; Catellani, A.; Galli, G. Water at a Hydrophilic Solid Surface Probed by Ab initio Molecular Dynamics: Inhomogeneous Thin Layers of Dense Fluid. *J. Am. Chem. Soc.* **2005**, *127*, 6830–6835, doi:10.1021/ja042963u.
20. Manzano, H.; Durgun, E.; López-Arbeloa, I.; Grossman, J. C. J. C. Insight on Tricalcium Silicate Hydration and Dissolution Mechanism from Molecular Simulations. *ACS Appl. Mater. Interfaces* **2015**, *7*, 14726–14733, doi:10.1021/acsami.5b02505.
21. Manzano, H.; Durgun, E.; Abdolhosseine Qomi, M. J.; Ulm, F.-J.; Pellenq, R. J. M.; Grossman, J. C. Impact of Chemical Impurities on the Crystalline Cement Clinker Phases Determined by Atomistic Simulations. *Cryst. Growth Des.* **2011**, *11*, 2964–2972, doi:10.1021/cg200212c.
22. Durgun, E.; Manzano, H.; Pellenq, R. J. M.; Grossman, J. C. Understanding and Controlling the Reactivity of the Calcium Silicate phases from First Principles. *Chem. Mater.* **2012**, *24*, 1262–1267, doi:10.1021/cm203127m.
23. Durgun, E.; Manzano, H.; Kumar, P. V. V; Grossman, J. C. J. C. The Characterization, Stability, and Reactivity of Synthetic Calcium Silicate Surfaces from First Principles. *J. Phys. Chem. C* **2014**, *118*, 15214–15219, doi:10.1021/jp408325f.
24. Huang, J.; Valenzano, L.; Singh, T. V.; Pandey, R.; Sant, G. Influence of (Al, Fe, Mg) Impurities on Triclinic Ca3SiO5: Interpretations from DFT Calculations. *Cryst. Growth Des.* **2014**, *14*, 2158–2171, doi:10.1021/cg401647f.
25. Huang, J.; Wang, B.; Yu, Y.; Valenzano, L.; Bauchy, M.; Sant, G. Electronic Origin of Doping-Induced Enhancements of Reactivity: Case Study of Tricalcium Silicate. *J. Phys. Chem. C* **2015**, *119*, 25991–25999, doi:10.1021/acs.jpcc.5b08286.
26. Mishra, R. K.; Flatt, R. J.; Heinz, H. Force Field for Tricalcium Silicate and Insight into Nanoscale Properties: Cleavage, Initial Hydration, and Adsorption of Organic Molecules. *J. Phys. Chem. C* **2013**, *117*, 10417–10432, doi:10.1021/jp312815g.
27. Wang, Q.; Guo, Y.; Manzano, H.; Lopez-Arbeloa, I.; Shen, X.; Li, F. First-principles study of water adsorption and dissociation on β-C2S (100). In *RILEM InternationalSymposium on Concrete Modeling-CONMOD 2014*; RILEM publications, 2014.
28. Wang, Q.; Manzano, H.; Guo, Y.; Lopez-Arbeloa, I.; Shen, X. Hydration Mechanism of Reactive and Passive Dicalcium Silicate Polymorphs from Molecular Simulations. *J. Phys. Chem. C* **2015**, *119*, 19869–19875, doi:10.1021/acs.jpcc.5b05257.
29. Wang, Q.; Li, F.; Shen, X.; Shi, W.; Li, X.; Guo, Y.; Xiong, S.; Zhu, Q. Relation between reactivity and electronic structure for α'L-, β- and γ-dicalcium silicate: A first-principles study. *Cem. Concr. Res.* **2014**, *57*, 28–32, doi:10.1016/j.cemconres.2013.12.004.
30. Mumme, W. G.; Hill, R. J.; Bushnellwye, G.; Segnit, E. R. Rietveld Crystal-Structure Refinements, Crystal-Chemistry and Calculated Powder Diffraction Data for the Polymorphs of Dicalcium Silicate and Related Phases. *Neues Jahrb. Fur Mineral.* **1995**, *169*, 35–68.
31. Delley, B. From molecules to solids with the DMol3 approach. *J. Chem. Phys.* **2000**, *113*, 7756–7764.
32. Perdew, J. P.; Burke, K.; Ernzerhof, M. Generalized gradient approximation made simple. *Phys. Rev. Lett.* **1996**, *77*, 3865–3868.
33. Monkhorst, H. J.; Pack, J. D. Special points for Brillouin-zone integrations. *Phys. Rev. B* **1976**, *13*, 5188–5192.
34. Neugebauer, J.; Scheffler, M. Adsorbate-substrate and adsorbate-adsorbate interactions of Na and K

adlayers on Al (111). *Phys. Rev. B* **1992**, *46*, 16067.

35. Momma, K.; Izumi, F. VESTA: a three-dimensional visualization system for electronic and structural analysis. *J. Appl. Crystallogr.* **2008**, *41*, 653–658, doi:10.1107/s0021889808012016.
36. Machesky, M. L.; Predota, M.; Wesolowski, D. J.; Vlcek, L.; Cummings, P. T.; Rosenqvist, J.; Ridley, M. K.; Kubicki, J. D.; Bandura, A. V; Kumar, N. Surface protonation at the rutile (110) interface: explicit incorporation of solvation structure within the refined MUSIC model framework. *Langmuir* **2008**, *24*, 12331–12339.
37. Allen, J. P.; Parker, S. C.; Price, D. W. Atomistic Simulation of the Surface Carbonation of Calcium and Magnesium Oxide Surfaces. *J. Phys. Chem. C* **2009**, *113*, 8320–8328, doi:10.1021/jp810885m.
38. Bolis, V.; Fubini, B.; Marchese, L.; Martra, G.; Costa, D. Hydrophilic and hydrophobic sites on dehydrated crystalline and amorphous silicas. *J. Chem. Soc. Faraday Trans.* **1991**, *87*, 497–505, doi:10.1039/FT9918700497.
39. Grabowski, S. J. Hydrogen bonding strength—measures based on geometric and topological parameters. *J. Phys. Org. Chem.* **2004**, *17*, 18–31, doi:10.1002/poc.685.
40. Duque-Redondo, E.; Manzano, H.; Epelde-Elezcano, N.; Martínez-Martínez, V.; López-Arbeloa, I. Molecular Forces Governing Shear and Tensile Failure in Clay-Dye Hybrid Materials. *Chem. Mater.* **2014**, *26*, 4338–4345, doi:10.1021/cm500661d.
41. Hirshfeld, F. L. Bonded-atom fragments for describing molecular charge densities. *Theor. Chim. Acta* **1977**, *44*, 129–138.
42. Grabowski, S. J. What Is the Covalency of Hydrogen Bonding? *Chem. Rev.* **2011**, *111*, 2597–2625, doi:10.1021/cr800346f.
43. Elgabarty, H.; Khaliullin, R. Z.; Kühne, T. D. Covalency of hydrogen bonds in liquid water can be probed by proton nuclear magnetic resonance experiments. *Nat. Commun.* **2015**, *6*.
44 Kerisit, S.; Bylaska, E. J.; Felmy, A. R. Water and carbon dioxide adsorption at olivine surfaces. *Chem. Geol.* **2013**, 359, 81–89.
45. Juilland, P.; Gallucci, E.; Flatt, R.; Scrivener, K. Dissolution theory applied to the induction period in alite hydration. *Cem. Concr. Res.* **2010**, *40*, 831–844, doi:10.1016/j.cemconres.2010.01.012.